RANS SIMULATIONS OF THE MULTIPHASE FLOW AROUND THE KCS HULLFORM

J B Banks (University of Southampton, UK)
A B Phillips (University of Southampton, UK)
P W Bull (QinetiQ Ltd, UK)
S R Turnock (University of Southampton, UK)

1. SUMMARY

A commercial RANS code is used to investigate the multiphase flow field surrounding the KCS hull form. Results are presented for the associated wave pattern (case 2.1), dynamic sinkage and trim (case 2.2b) and self propulsion parameters for the hull using a body force propeller model (case 2.3a).

2. INTRODUCTION

Traditionally the resistance of ships has been determined using towing tank experiments. Over the past two decades increased computational power has allowed numerical approaches to replicate and potentially start to replace towing tank experiments. This work investigates the quality of results that can be achieved using a commercial Reynolds Averaged Navier Stokes (RANS) flow solver, ANSYS CFX Version 12 (ANSYS, 2009). This work is a contribution to the Gothenburg 2010 workshop on CFD in ship hydrodynamics and compares the results from CFD based methods with model tests performed by participating towing tanks on the KRISO Container Ship (KCS).

Fig.1 KCS hull form

3. THEORETICAL APPROACH

A finite volume method, using a Volume of Fluid (VOF) approach was used. This method is derived from the surface integration of the conservative form of Navier Stokes' equations over a control volume. Equations (1) and (2) are the incompressible Reynolds averaged Navier-Stokes (RANS) equations in tensor form and Equation (3) is the volume fraction transport equation (Peric and Ferziger, 2002).

$$\frac{\partial(\rho U_i)}{\partial t}+\frac{\partial(\rho U_i U_j)}{\partial x_j}=-\frac{\partial P}{\partial x_i}+\frac{\partial}{\partial x_j}\left[\mu\left(\frac{\partial U_i}{\partial x_j}+\frac{\partial U_j}{\partial x_j}\right)\right] -\frac{\partial}{\partial x_j}\left(\rho\overline{u'_i u'_j}\right)+f_i \quad (1)$$

$$\frac{\partial U_i}{\partial x_i}=0 \quad (2) \qquad \frac{\partial c}{\partial t}+\frac{\partial(cU_j)}{\partial x_j}=0 \quad (3)$$

The volume fraction c is defined as (V_{air}/V_{total}) and the fluid density, ρ, and viscosity, μ, are calculated as $\rho=\rho_{air}c+\rho_{water}(1-c)$ and $\mu=\mu_{air}c+\mu_{water}(1-c)$. External forces applied to the fluid are represented as f_i, which include buoyancy forces and momentum sources representing the influence of a propeller. The effect of turbulence is represented in (2) by the Reynolds stress tensor $\rho\overline{u'_i u'_j}$ and is modelled using a turbulence model.

3.1 Turbulence modelling

Both a Shear Stress Transport (SST) eddy viscosity model and a Baseline (BSL) Reynolds stress model (ANSYS, 2009) were used to evaluate the Reynolds stress tensor.

Case	Description	Turbulence model
2.1	Wave pattern	SST & BSL
2.2b	Sinkage and trim	SST
2.3a	Self propelled	SST

The SST model blends a variant of the k-ω model in the inner boundary layer and a transformed version of the k-ε model in the outer boundary layer and the free stream (Menter, 1994). This has been shown to be better at replicating the flow around the stern of a ship, than simpler models such as k-ε, single and zero equation models (Larsson *et al*, 2000)(Hino, 2005). The BSL Reynolds stress model includes transport equations for each component of the Reynolds stress tensor. This allows anisotropic turbulence effects to be modelled helping to model complex flow features such as separation off curved surfaces (Peric and Ferziger, 2002). The BSL model is blend of a Reynolds stress-ω model for the inner boundary layer and ε based in the outer and free stream (Bull, 2005).

3.2 Sinkage and Trim

To capture the sinkage and trim experienced by a vessel travelling at a forward speed, the surface mesh representing the hull was displaced based on the total heave force and pitching moment acting on the vessel and the vessels water plane area and moment to change trim. This was achieved using CFXs in built "mesh morphing" model which is used to calculate the new node locations throughout the fluid domain at each time step, while maintaining mesh topology. The resulting vessel orientation has no net heave force or pitching moment.

3.3 Propeller models

To reduce the computational cost associated with self propulsion simulations a body force propeller model was used. This represents the impact of the propeller on the fluid as a series of axial and tangential momentum source terms, fb_x and fb_θ respectively. These are calculated using the Hough and Ordway Thrust and Torque distribution (Hough, 1965), as was implemented by (Stern *et* al, 1988). A detailed description of the methodology adopted here is presented in (Phillips *et al*, 2010).

The momentum source terms were calculated based on the propeller rps (n), the open water propeller characteristics and the inflow velocity field providing the mean wake fraction $\bar{W}_t$, which is assumed to be equal to the Taylor wake fraction w_t.

Initially no momentum sources were applied, by setting n=0, providing the initial flow field entering the propeller domain. Once the convergence criteria were met the velocity components

entering the propeller disk are sampled providing the wake fraction. This is then used along with an initial estimate of n=9 to calculate the thrust and torque generated by the propeller, which are represented by axial and tangential momentum source terms. The rps is then iteratively varied using a Secant method (each time convergence is achieved) until;

$$|\text{Thrust} - \text{Drag} + \text{SFC}| < 1 \text{ N}.$$

4. NUMERICAL MODEL

Table 1 Numerical simulation properties.

Property	**SOTON**	**QINETIQ**
Half mesh No. of elements	~ 10M	~9M
y+ on the hull	~ 1 (max value 1.2)	< 10
Domain Physics	Homogeneous Water/Air multiphase, SST or BSL turbulence model, Automatic wall function, Buoyancy model –density difference, Standard free surface model	
Boundary physics:		
Inlet	Defined volume fraction and flow speed	
	Turb. Intensity= 0.05	Zero gradient
Outlet	Opening with entrainment with relative pressure = hydrostatic pressure	
Bottom/side wall	Wall with free slip condition	Outlets with hydrostatic pressure
Top	Opening with entrainment with relative pressure 0 Pa	
Hull	Wall with no slip condition	
Symmetry plane	Along centreline of the hull	
Solver settings:		
Advection scheme	High Resolution (ANSYS, 2009)	
Timescale control	Physical timescale function: 0.01[s] + 0.09[s]*step(atstep-20)+ 0.1[s]*step(atstep-200)	$0.03\left(\frac{L_{pp}}{Fn\sqrt{gL_{pp}}}\right)$
Convergence criteria	Residuary type: RMS	
	Target: 1e-5	Target: 1e-6
Multiphase control	Volume fraction coupling	
Processing Parameters:		
Computing System	Iridis 3 Linux Cluster (University of Southampton)	Linux cluster (QinetiQ Haslar)
Run type	Parallel (24 Partitions run on 3x8 core nodes each with 23 Gb RAM)	Parallel(up to 64 Partitions run on 8x8 core nodes each with 8 Gb RAM)

Simulations are performed using ANSYS CFX V12 (ANSYS, 2009). This is a commercial finite volume code, which uses collocated (nonstaggered) grids for all transport equations, coupling pressure and velocity using an interpolation scheme. The physical parameters and solver settings used to define the numerical solution are provided in Table 1, along with details of the computing resources used for the largest mesh.

5. MESHING TECHNIQUE

5.1 Wave Pattern (Case 2.1) - Southampton

A structured mesh was built using ANSYS ICEM around the full scale KCS hull geometry. The domain width and depth matched the dimensions of one half of the KRISO towing tank. The length was selected to allow one ship length in front of the hull and two behind. This was then converted to model scale dimensions each time a mesh was generated.

A blocking structure was developed that allowed a good quality surface mesh to be created over the hull (see Figure 1). It was found that collapsing the blocks under the stern down to a point provided the best overall mesh structure in this region. This approach allowed extra mesh density to be added in this localised area where large surface curvatures needed to be captured. Elements were also clustered within the region of the free surface to allow a sharp interface to be captured.

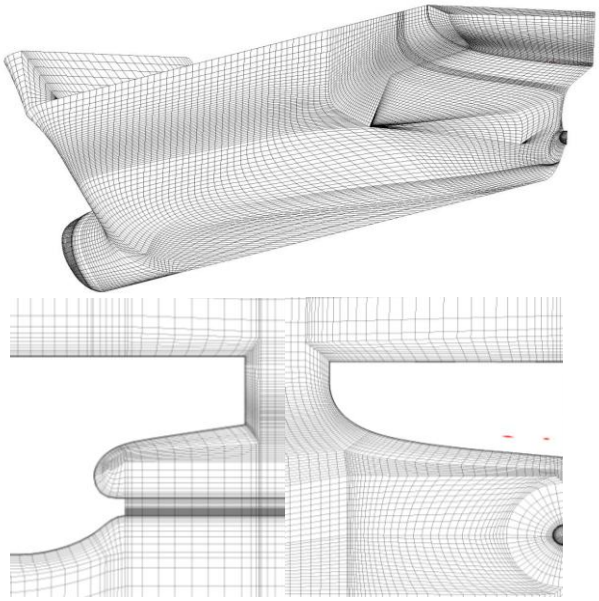

Fig.2 SOTON: Hull surface mesh structure (top), O-grid structure at stern from the side (left) and from the stern (right), for the initial mesh containing 0.8M elements.

Once satisfied with the surface mesh structure an O-grid blocking structure was grown out from the surface of the hull. The depth of the inner O-grid was matched to approximately that of the maximum expected boundary layer. Another outer O-grid was then created so as to provide a smooth transition between the near wall radial mesh and the far field Cartesian structure. Another key feature is the continuation of the O-grids about the propeller axis, towards the outlet of the domain. The outer O-grid was expanded to match the propeller diameter allowing a propeller model to be easily added later. Two splits were also placed within the outer domain blocking structure, one behind the hull and one offset from the hull centreline. This allowed the regions of high mesh density to be forced onto the free surface both on the hull surface and in the outer domain.

A half body mesh of 10M elements was produced with two $\sqrt{2}$ global mesh reductions, providing 4M and 1.5M element meshes, each with a y^+ of 1 over the hull. More details of this process can be found in (Banks et al, 2010).

5.2 Wave Pattern (Case 2.1) QinetiQ

In a similar manner, a structured mesh was built using ANSYS ICEM around the full scale KCS hull geometry. The domain length, width and depth were chosen based on the ship length with one ship length in front of the hull and two behind. The top and bottom of the domain were defined as one ship length below and a half ship length above the keel line, whilst the width was 1.3 ship lengths (see Fig.3).

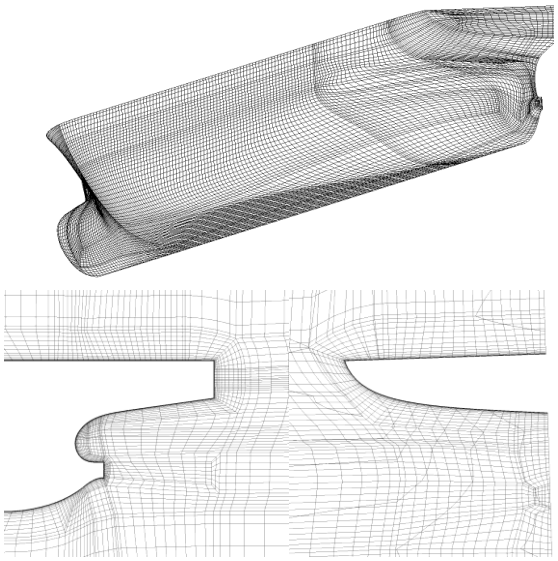

Fig.3 QINETIQ: Hull surface mesh structure (top), O-grid structure at stern from the side (left) and from the stern (right), for the coarsest mesh containing 1M elements.

The topological structure of the O-grids on the hull was defined to give a near uniform, quadrilateral surface grid on the hull surface for the baseline grids but with some control within the free-surface region. A small O-grid was also placed downstream of the propulsor hub which extended to just aft of the transom. The first cell height for the O-grid around the hull was chosen to give $y^+ < 10$ for the model scale flow Reynolds number.

Two sequences of grids were generated based on grid topologies with 4M and 5M cells. Finer and coarser grids were produced using global element refinement factors of 1.25 and 0.8 respectively to give a series of grids with 1M, 2M, 2.5M, 4M, 5M, 6.8M and 9M computation cells. Each of the grid spacings perpendicular to the outer boundaries of the domain were adjusted for the coarsest grids to provide smooth expansion rates.

5.3 Sinkage and Trim (Case 2.2b) – QinetiQ

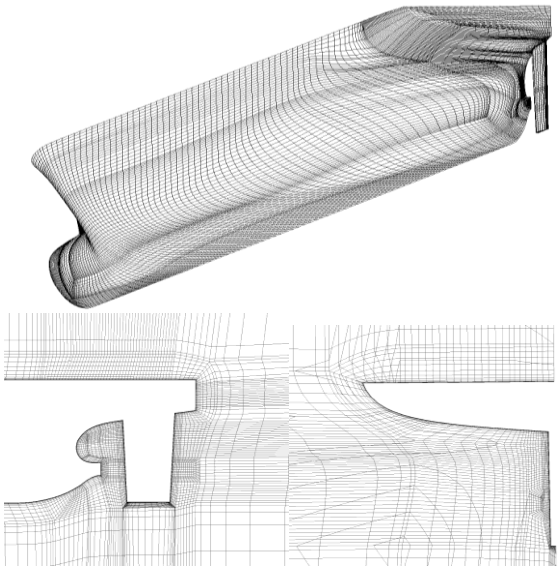

Fig.4 QINETIQ: Hull with rudder surface mesh structure (top), O-grid structure at stern from the side (left) and from the stern (right), for the coarse mesh containing 1M elements.

The rudder was included in the geometry definition for the ANSYS ICEM mesh generation process. Additional vertical splits were created in the overall topology for the 4M cell baseline grid which corresponded to the leading and trailing edge of the rudder and additional O-grid topologies were placed around the rudder. Additional grid points were required in the overall topology to resolve the rudder geometry, and its boundary layer, increasing the baseline grid from 4M cells to 5M cells.

Finer and coarser grids were produced using global element refinement factors of 1.25 and 0.8 respectively to give a series of grids with 680K, 1M, 1.7M, 3M, 5M and 9M computation cells.

5.4 Self propelled (Case 2.3a)

To incorporate a propeller model a separate cylindrical mesh was inserted into the Southampton mesh in the position of the propeller. The mesh density in the outer O-grid was increased to provide a higher mesh resolution entering and leaving the propeller domain. Due to the intrinsic asymmetry in self propelled simulations the entire domain had to be modelled by mirroring the half body mesh. As this doubles the total mesh density a further $\sqrt{2}$ mesh reduction was conducted to minimize computing requirements. This resulted in three half body meshes of 0.75M, 1.7M and 4.5M elements.

6. MESH SENSITIVITY STUDY

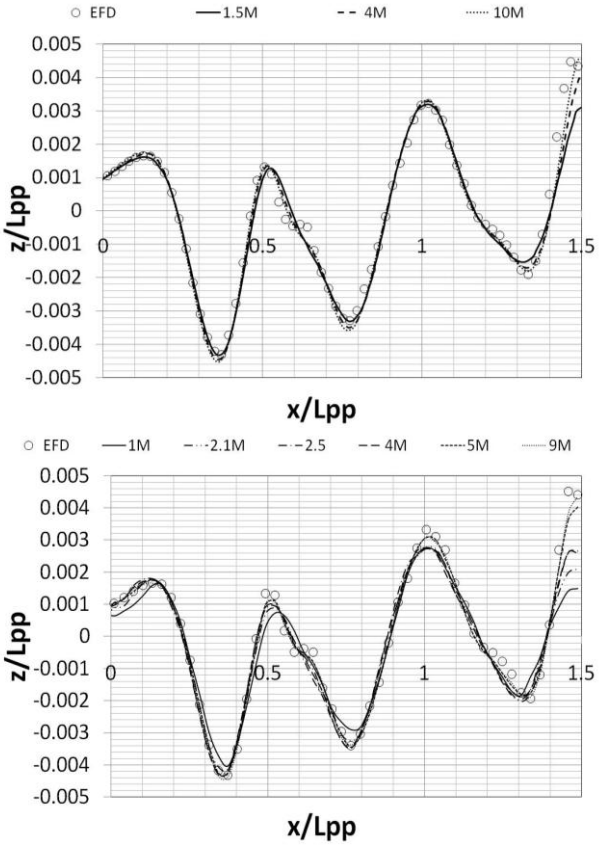

Fig.5 Comparison between experimental (EFD) and CFD wave elevation at a distance of y/Lpp=0.15 from the ship centreline at Fn=0.26. Southampton results (top), QinetiQ results (bottom). The Forward perpendicular is positioned at x/Lpp=0.

To observe the impact of mesh density on the different mesh structures (Southampton Vs QinetiQ) a wave cut profile, using the BSL turbulence model, was compared with EFD data for each of the different mesh densities (Fig.5). It can be seen that both of the mesh structures display significant sensitivity to mesh density astern of the hull, particularly at the next wave peak (x/Lpp = 1.5). However, over the rest of the observed wave cut we see good convergence between the highest mesh densities as well as with EFD data.

7. COMPARISON OF BSL WAVE PATTERN DATA (CASE 2.1)

To asses the influence of different meshes and numerical models a comparison of the wave pattern data obtained using the BSL Reynolds stress turbulence model from case 2.1 was made. In Fig.6 it can be seen that in both cases the global wave pattern shows good correlation to the EFD surface plot. Some variation is observed in the size of the stern wave leaving the transom and magnitude of the stern wave pattern further down stream of the hull. These can be directly compared in the wave cut profile.

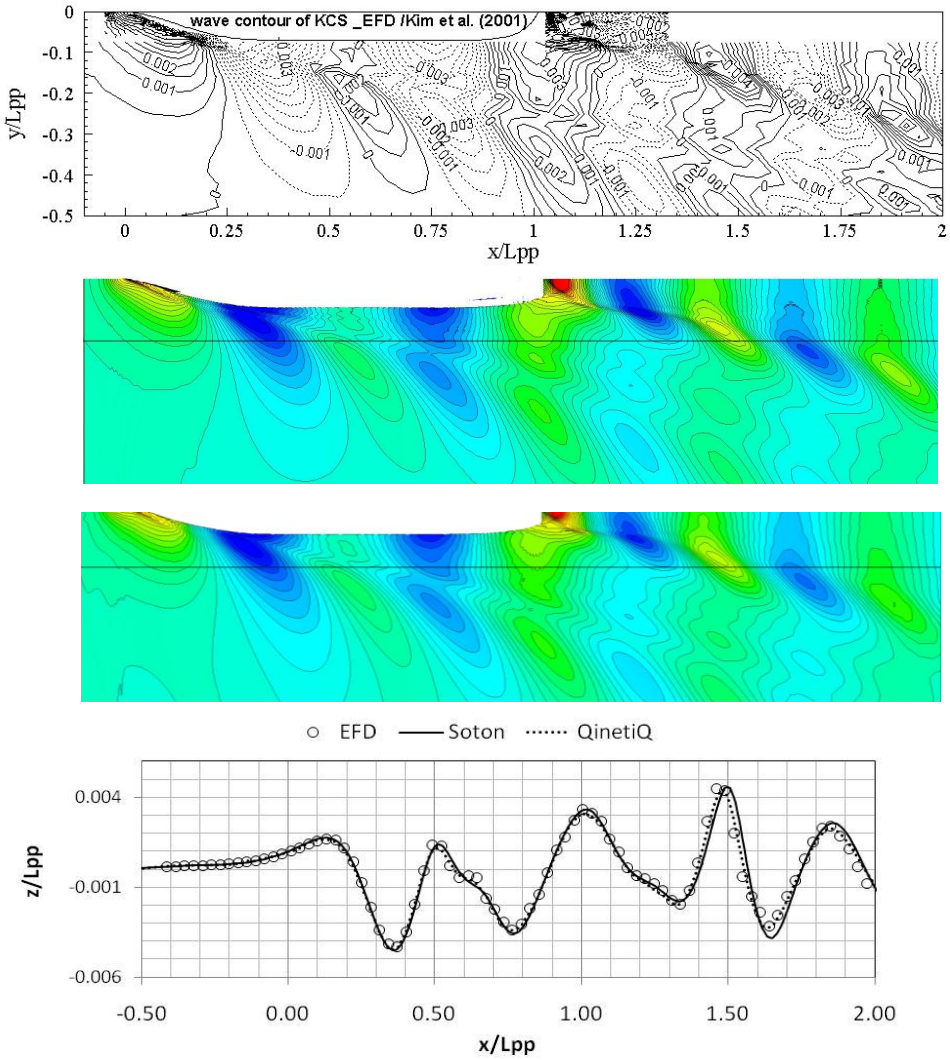

Fig.6 Free surface elevation, z/Lpp, of global wave pattern, at Fn=0.26, for (Top Down) Experimental data, SOTON CFD results and QinetiQ CFD results. Contours range from z/Lpp = -0.005 to 0.010 in steps of 0.0005. The straight lines represent the positions of the wave cut at y/Lpp= 0.15 which are plotted against EFD data for both meshes (Bottom).

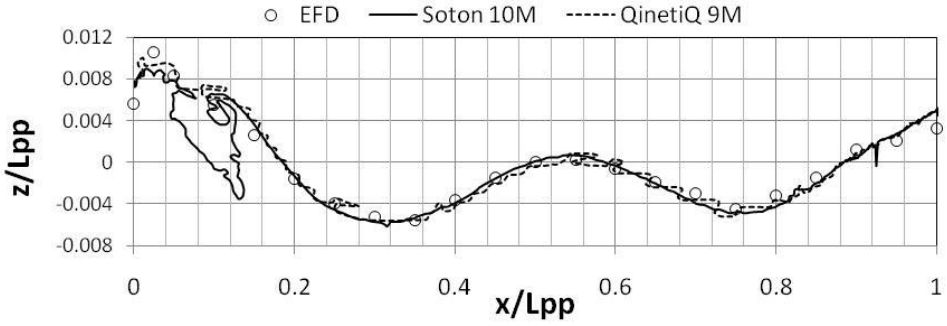

Fig.7 Comparison of free surface elevation along the surface of the hull plotted agaings EFD data at Fn=0.26.

In Fig.7 we can see that in both cases the free surface along the hull appears irregular with the Southampton results showing large gapes and drops in the free surface caused by air pockets on the hull surface near the bow and stern. This ventilation problem was also observed by QinetiQ whilst using a y^+ of 1 but was improved by increasing it to 5-10. It can be seen that this resulted in a more continuous free surface along the hull but with increased smaller undulations along its length.

The components of resistance obtained by both the Southampton and QinetiQ simulations for case 2.1 are also compared to the experimental data provided in (Kim *et al*, 2001) in Table 2. The static wetted surface area used in the calculation of force components was 9.5121 m^2. It can be seen that both turbulence models used by QinetiQ provided total resistances that agree closely with the experimental data, with the BSL model providing a slightly better match with the frictional and pressure components. The Southampton results, however, appear to over estimate all components of resistance, despite significant improvement being made to the pressure component using the BSL turbulence model. One of the factors contributing to this could be the increased air resistance due to the Southampton mesh containing the full topside geometry of the hull, see Fig.2 and Fig.3. Although air resistance is normally assumed small enough to neglect, it appears to be making up 2 – 5% of the total resistance and therefore potentially needs to be accurately modelled so as to match the experimental procedure.

Table 2 Comparison of Resistance Components.

Mesh	Turbulence model	CT ($x10^3$)	CF ($x10^3$)	CP ($x10^3$)
Soton	SST	3.96	3.04	0.92
Soton	BSL	3.79	3.01	0.78
QinetiQ	SST	3.61	2.95	0.67
QinetiQ	BSL	3.60	2.87	0.73
Experimental		3.56		
Calculated from ITTC Procedure			2.83	0.73

8. SINKAGE AND TRIM - CASE 2.2B

In each simulation the hull geometry was fixed in position for the first 1000 timesteps to allow the fluid forces and moments to converge. From this point the hull is free to heave and trim for another 1000 timesteps or until convergence is reached. An example time history of this process is given in Fig.8, whereas the close correlation with the EFD data over the Froude number range can be seen in Fig.9.

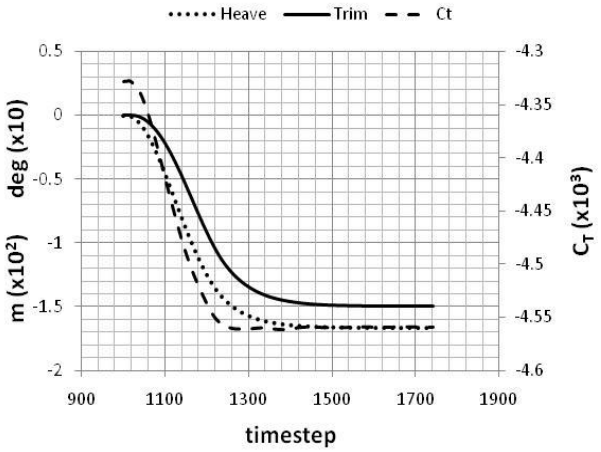

Fig.8 Example time history of a sinkage and trim simulation for Fn = 0.2816 using the finest mesh (9M).

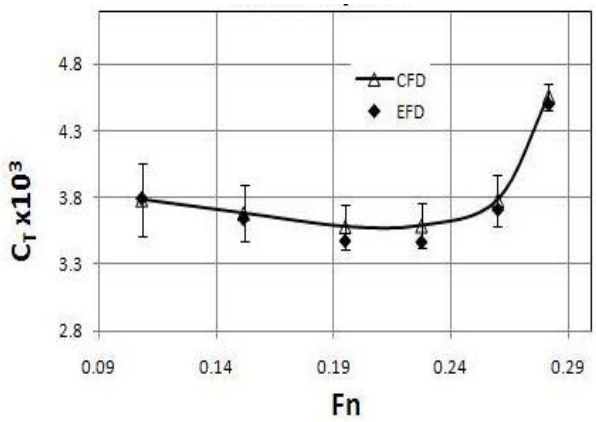

Fig.9 Comparison of EFD and CFD variation of total resistance with Froude number, with numerical uncertainty error bars.

8.1 Uncertainty analysis

The procedure adopted is presented in (Eca &Hoeksra, 2008). The experimental values for each mesh density were determined as the mean value over the last 200 iterations, with the standard deviation providing the iterative uncertainty U_I. The least squares fit to the data was conducted in Matlab assuming a grid ratio of 1.2.

9. SELF PROPELED – CASE 2.3A

Table 3 Resistance propeller parameters for self propulsion at ship point.

Parameters	EFD	Coarse (1.5M)	Medium (3.4M)	Fine (9M)
$CT\times10^3$	4.162	4.344	4.321	4.287
$CF\times10^3$		2.903	2.959	2.988
$CP\times10^3$		1.441	1.362	1.300
K_T	0.170	0.200	0.199	0.202
K_Q	0.0288	0.034	0.033	0.034
w_T	0.208	0.281	0.279	0.296
n (rps) (for given SFC)	9.5	9.463	9.464	9.358

The results presented in Table 3 show noticeable discrepancies between the numerical and experimental results. The reason for this is two fold. The wake into the propeller plane has not been accurately captured, (see w_T values in Table 3) this has reduced the propeller advance coefficient value and thus increased the K_T and K_Q predicted from the open water curves. However, since the drag is also over predicted the required thrust is increased which causes the predicted rps to be nearly correct. However, while the results presented are less than ideal the methodology appears to work and provides a simple method of replicating the propeller forces and calculating the self propulsion parameters. However, further effort is required to ensure that the vessel drag and wake fraction are correctly predicted.

Fig.10 illustrates the velocity components downstream of the propeller. Variation in the axial component can be attributed to not replicating the hub geometry and the over prediction of thrust. The asymmetry is not captured due to the non-uniform inflow into the propeller plane not being included in the body force model.

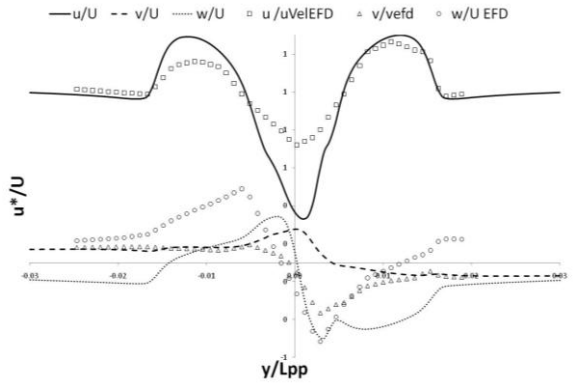

Fig.10 Velocity components down stream of propeller (x/Lpp=0.911, z/Lpp = -0.03)

10. DISSCUSION

10.1 Differences in Mesh structure

The main difference appears to be the surface mesh structure created on the hull. To accommodate the complex geometry of the KCS stern sections the QinetiQ mesh uses multiple O-grids to create a complex mesh structure localised to the hull surface. This leaves a relatively simple mesh structure in the outer domain. In contrast, the surface structure created in the SOTON mesh is maintained throughout the rest of the domain.

Apart from comparing the fundamental mesh structure it is important to assess how the elements are distributed in the two different meshes. Table 4 provides details of how the elements are distributed over different regions in the mesh. It should be noted that although both meshes leave 1xLpp ahead and 2xLpp astern of the hull the width and depth of the domains vary leading to different volumes.

An immediate observation is that the QinetiQ mesh places more cells ahead and along the waterline of the hull. Whereas the Southampton mesh, despite having a smaller free surface area, places more cells here, especially astern of the hull. Another important observation is the increase in hull surface and waterline nodes in case 2.2b due to the addition of the rudder.

Table 4 Comparison of mesh distribution.

Number of grid nodes in location:	Case 2.1		Case 2.2b
	Soton	QinetiQ	QinetiQ
Total in half hull domain	10312611	8791499	9251577
In hull O-grid	1694265	1354698	1354698
On static Free Surface	71504	66710	56056
Distribution ahead of hull	40	62	62
Distribution behind hull	101	67	67
Distribution to side of hull	80	76	76
Hull surface	64237	52827	77313
Along Static Waterline	366	396	434
Along hull midgirth (BWL)	97	74	118
Along hull midgirth (AWL)	40	26	27

10.2 Turbulence modelling

Both groups found that the BSL Reynolds stress model provided noticeably superior results for both the free surface deformation and components of resistance for case 2.1. Ideally this would also have been used in both cases 2.2b and 2.3a, however, reduced numerical stability made this impractical.

11. CONCLUSION

Numerical simulations of the KCS hull form are presented as part of the work jointly submitted by the University of Southampton and QinetiQ Ltd to the Gothenburg 2010 workshop. Despite the differences in meshing technique and numerical setup the wave pattern data obtained shows good correlation to each other and the experimental data. Simple and effective methods for modelling both the dynamic sinkage and trim, and the propeller behind a ship, have been implemented. However a greater level of detail is needed in the propeller inflow to achieve accurate self propelled results.

Both parties experienced problems with air ventilation on the wetted surface of the hull. It was found that this could be significantly reduced by increasing the y^+ from 1 to 5-10.

Another interesting finding was that when the entire topside hull geometry was modelled the air drag equated to 2-5% of the total hull drag, raising into question the common assumption that the air phase can be neglected in CFD simulations. Additional information about the experimental procedure regarding the air drag and the above water structure would enable validation of this component.

REFERENCES

ANSYS. (2009) ANSYS CFX, Release 12.0. ANSYS.

Banks, J., Phillips, A. B., Turnock, S. R., (2010) Free-surface CFD Prediction of Components of Ship Resistance for KCS, 13th Numerical Towing Tank Symposium, Duisburg, Germany.

Bull, P.W., (2005) Verification and Validation of KVLCC2M Tanker Flow, CFD Workshop Tokyo 2005.

Eca, L., Hoekstra, M., (2008) Testing Uncertainty Estimation and Validation Procedures in the Flow Around a Backward Facing Step, 3rd Workshop on CFD Uncertainty Analysis, Lisbon.

Hino T. (2005) CFD Workshop Tokyo 2005. In: The Proceedings of CFD Workshop Tokyo.

Hough, G.R., Ordway, D.E., The generalised actuator disc, Developments in Theoretical and Applied Mechanics, Vol 2, pp 317–336.

Kim, W.J., Van, D.H. and Kim, D.H., (2001) Measurement of flows around modern commercial ship models, Exp. in Fluids, Vol. 31, pp 567-578

Larsson L, Stern F, Bertram V. (2003) Benchmarking of Computational Fluid Dynamics for Ship Flows: The Gothenburg 2000 Workshop. Journal of Ship Research 2003, Vol47, pp 63–81.

Menter, F.R., (1994) Two-equation eddy-viscosity turbulence models for engineering applications. AIAA Journal, Vol 32, pp 1598 –605.

Peric, M., Ferziger, J.H., (2002) Computational Methods for Fluid Dynamics, Springer, 3rd edition.

Phillips, A.B., Turnock, S.R. and Furlong, M.E. (2010) Accurate capture of rudder-propeller interaction using a coupled blade element momentum-RANS approach. *Ship Technology Research (Schiffstechnik)*, Vol 57, pp 128-139.

Stern, F., Kim, H.T., Patel, N.M., Chen, H.C., (1988) A Viscous-Flow Approach to the Computation of Propeller-Hull Interaction. Journal of Ship Research , Vol 32, pp 246–262.